

Prompt neutron emission from spontaneous fission of ^{252}Cf at long times

K. Skarsvåg

Institutt for Atomenergi, Kjeller Research Establishment, 2007 Kjeller, Norway

(Received 12 July 1977)

A search for neutron emission from spontaneous fission of ^{252}Cf in the time range 10^{-15} – 10^{-8} s has been made by a method based upon the solid angle aberration. No positive evidence for neutron emission in this time range has been found, but an upper limit for the relative intensity of a single long-lived component as a function of its mean lifetime has been set. It is concluded that very few if any neutrons are emitted with mean lifetimes longer than 10^{-13} s, but possibly there is a sizable fraction with a mean lifetime in the 10^{-14} s range. A competition between neutron and γ -ray emission can therefore possibly take place in the time region 10^{-14} – 10^{-13} s after fission, as can be expected at excitation energies near the yrast levels.

[RADIOACTIVITY ^{252}Cf (sf); measured upper limit of I_n ($t = 10^{-15}$ – 10^{-8} s).]

I. INTRODUCTION

It is generally assumed that the bulk of the prompt neutrons from fission are emitted at very short times^{1,2} (of the order of 10^{-21} – 10^{-17} s). It cannot be ignored, however, that at excitation energies near the yrast levels³ neutrons can be emitted at much later times, and that some of the faster⁴ γ -ray transitions (at times of the order of 10^{-14} – 10^{-13} s) actually occur before all the neutrons are emitted. The experimental evidence for neutron emission in the nanosecond range⁵ has been questioned,⁶ and a more recent experiment⁷ does not confirm the existence of neutron emission in this time range.

A technique based upon the solid angle aberration can be applied not only to γ rays,⁴ but possibly also to neutrons. With a source on a thick backing a forward-backward anisotropy of neutrons relative to the fragments in flight arises from the slowing down of the fragments in the backing if the neutron emission times are not much smaller than the slowing-down times of the fragments. In a classical experiment⁸ the counting rates of neutrons in the forward and backward directions were shown to be equal within 2%, from which an upper limit of the time of emission of neutrons of 4×10^{-14} s was estimated.

The present experiment was designed to measure the forward-backward anisotropy of neutrons with an error smaller than 0.1%, in which case components with emission times in the range 10^{-15} – 10^{-8} s can be detected.

II. EXPERIMENTAL METHOD

The forward-backward anisotropy at an angle $\theta = 0^\circ$ will be defined here as

$$A = [W(0^\circ) - W(180^\circ)] / [W(0^\circ) + W(180^\circ)], \quad (1)$$

where $W(0^\circ)$ and $W(180^\circ)$ are the counting rates with the source on a thick backing facing and turning away from the neutron detector, respectively. The anisotropy A is a sum of several terms. The term A_D which arises from the solid angle aberration has been calculated for infinite and finite distance between source and fragment detector. The calculation has been based upon a model (fit 1 in Ref. 2) tested on experimental data for velocity (or energy) and angular distributions of prompt neutrons,⁹ with the additional assumption that the fully accelerated fragments have a long-lived component with mean lifetime τ and relative intensity c_r (with the index r for retarded). In Fig. 1 the anisotropy A_D for a source on nickel backing integrated from 0° to 30° and for a relative intensity $c_r = 0.1$ is plotted versus the decay constant λ ($\lambda = 1/\tau$) for different energy intervals. Here and in the following a value of 0.6 ps for the characteristic slowing-down time of fragments in nickel will be adopted. It should be noted that a large fraction of the low-energy neutrons is coming from the fragments going in the opposite direction. The anisotropy integrated over the whole or most of the energy range (0.18–10.4 MeV) can be assumed to be fairly model independent, and is rather large over a lifetime range of about six decades.

The anisotropy term A_s due to the change in solid angle of the neutron detector as seen from the fragments in flight (cf. Ref. 4) can be neglected except for the longer lifetimes.

The anisotropy term A_a caused by the penetration of the fragments into the backing (cf. Ref. 4) is in most cases several orders of magnitude smaller than the anisotropy due to the solid angle aberration A_D , and will be neglected here.

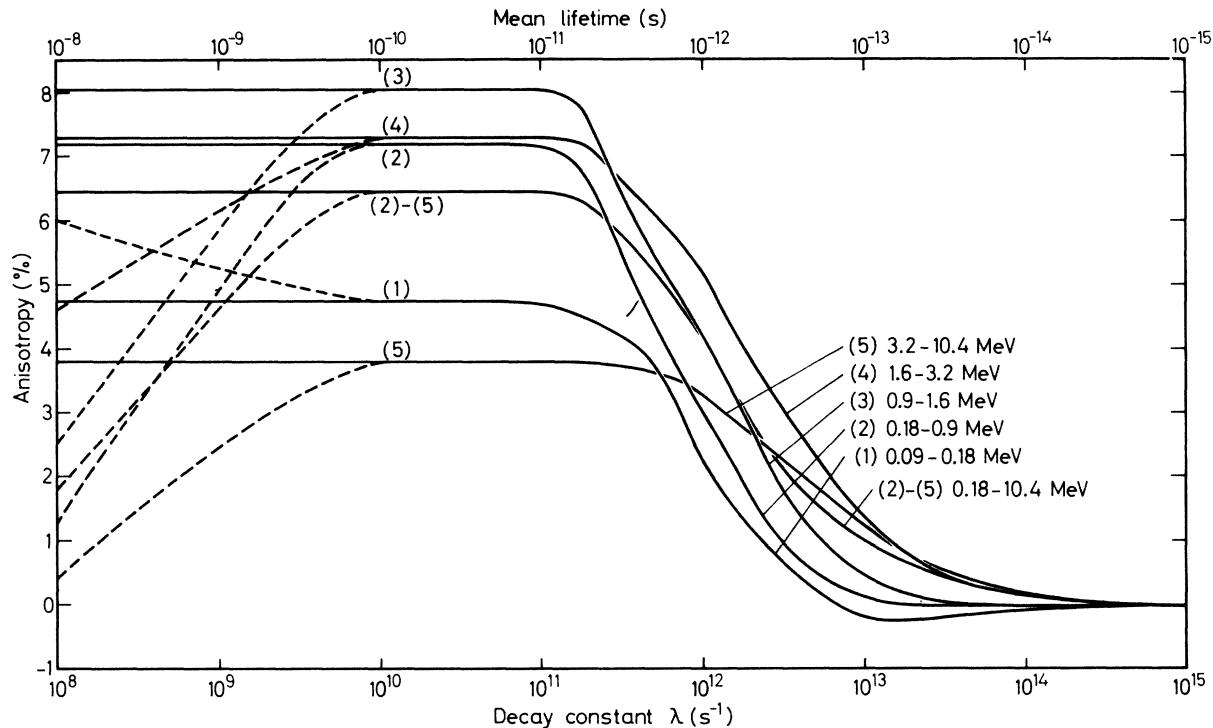


FIG. 1. The anisotropy A_D for a source on a nickel backing integrated from 0° to 30° and for a relative intensity $c_r = 0.1$ versus the decay constant λ , labeled in terms of energy intervals. The distance between source and detector is infinite (solid curves) or 1.2 cm (dashed curves).

III. EXPERIMENTAL SETUP

The experimental arrangement is shown in Fig. 2. This distance between the ^{252}Cf source and the face of the neutron detector was 96.6 (or 196.6) cm. The vacuum chamber with the source and the fission fragment detector was mounted on a turntable. Measurements were done for two fixed positions of the turntable, with the source on the thick backing facing the neutron detector (0°), and with the source turning away from it (180°). The horizontal position of the backing of the source (in the direction of the neutron detector), as viewed in a cathetometer, was adjusted to be the same for the two positions of the turntable. The ^{252}Cf source had a strength of about 10^5 fissions/min and was deposited on a nickel backing 22 mg/cm^2 thick. The fragment detector, which was an Ortec transmission mount detector 150 mm^2 in area and $208 \mu\text{m}$ (48 mg/cm^2) thick, was mounted at a distance of 1.2 cm from the source subtending a half-angle of 30° . The detector was in thermal contact with a cold finger which was kept at a temperature of -18°C by a Peltier module. The difference in attenuation of neutrons in the silicon wafer at 0° and the nickel backing at 180° was partly compensated for by the attenuation in an aluminium foil (26 mg/cm^2 thick) behind the backing. The vacuum cham-

ber had thin windows on the front and the back, each consisting of a Mylar foil $190 \mu\text{m}$ thick and an aluminium foil $30 \mu\text{m}$ thick. The neutron detector was a NE102A plastic scintillator optically coupled to a XP1040 photomultiplier. The scintillator was 17.9 cm in diameter and 7.5 cm thick and had a concentric cylindrical hole, 9.0 cm in diameter, which accommodated a boron plug¹⁰ (88 g of weight with 92% ^{10}B). To minimize the anisotropy caused by delayed γ rays,⁴ the detector was shielded on the front by a 2 cm thick lead shield and a 1 cm

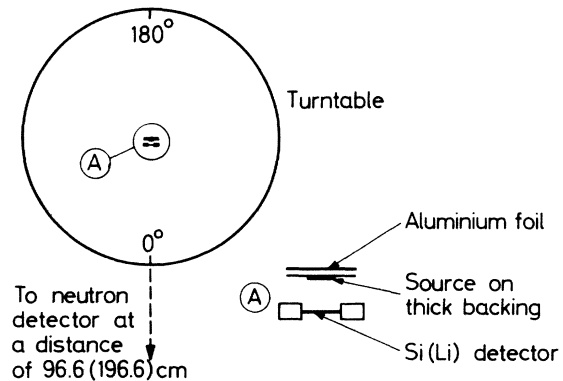


FIG. 2. Schematic diagram of experimental setup.

thick brass plate.

The bias of the plastic scintillator detector was set at the ^{241}Am 60 keV γ -ray peak. The time distribution over the given flight path was measured by a time-to-amplitude assembly. The time range was set to cover energies down to 90 keV. From a comparison of the time distributions of runs with the flight paths referred to above, it was concluded that the low-energy part below about 0.18 MeV was distorted by scattered neutrons, especially for the longer flight path. The main run was therefore made with the shorter flight path with 1 channel = 2.94 ns. The turntable automatically changed from one position to the other after a definite length of time (1000 s). Two time-of-flight distributions gated by the heavy and the light fragment peak, respectively, were recorded at the two angles in a 4×100 channel analyzer. The experiment was run for 23 days, and the total number of events was 4×10^6 .

IV. ANALYSIS AND RESULTS

The analysis is done in several steps. The first step is to correct for the background which was taken as the average of 4 channels for negative

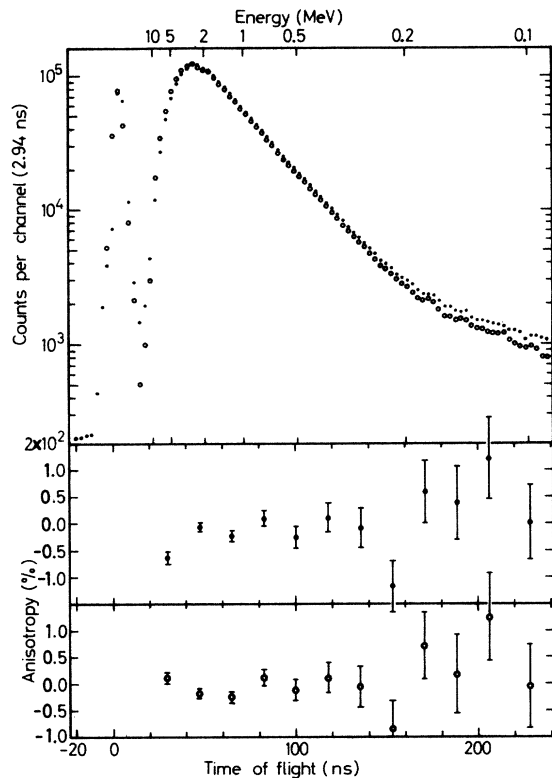


FIG. 3. Time distributions (at 0°) and anisotropies (six and six channels added together), uncorrected data (dots), and after the fourth step of correction (circles).

TABLE I. Forward-backward anisotropies of prompt neutrons.

Description	Anisotropy (%)
Raw data (0.18–10.4 MeV)	-0.204 ± 0.051
When corrected for background	-0.205
When corrected for time zero shift	-0.207
When corrected for resolution	-0.141
When corrected for attenuation	-0.099
When corrected for detector efficiency	-0.090 ± 0.072

times, and which on the average was about 0.8% of the total.

The time distributions at angles $\theta = 0^\circ$ and 180° are the sum of two distributions $W(\theta) = W_H(\theta) + W_L(\theta)$, where the index H (or L) refers to the fragment (heavy or light) which is counted. It should be stressed that there will be a difference in time zero and also in the resolution function in the time distributions gated by the heavy fragments on one side and the distributions gated by the light fragments on the other side. The difference arises over the fragment flight path and in the electronic triggering. The time zero T_{oF} ($F = H, L$) and the dispersion in time for constant distance Δt_F full width at half-maximum (FWHM) have been found to be independent of angle and are taken from a least-squares fit of the prompt γ -ray peaks with the data at 0° and 180° added together ($T_{oH} = 19.292$ channel, $T_{oL} = 19.446$ channel, $\Delta t_H = 1.60$ channel, $\Delta t_L = 1.18$ channel, where 1 channel = 2.94 ns). The second step is then to shift the time distributions by the fraction of a channel necessary to get the prompt γ -ray peak in the middle of a channel, where $T_{oL} - T_{oH} = 0.154$ channel. The total dispersion of the flight time includes the dispersion in time for constant distance and the dispersion due to the finite thickness of the scintillator. In the third step three and three channels are lumped together. In order to avoid spurious effects the data at 0° and 180° are added together [$W_{FS} = W_F(0^\circ) + W_F(180^\circ)$, $F = H, L$], transformed by the inverse response matrix, and finally divided between 0° and 180° in the same proportion as before the transformation.

In the fourth step the difference in the attenuation in the forward and backward directions is corrected for by means of the neutron cross sections.¹¹ In the fifth step the data are weighted by the inverse detector efficiency, which is found from the present and tabulated data⁹ through the model.² Anisotropies and time distributions (uncorrected

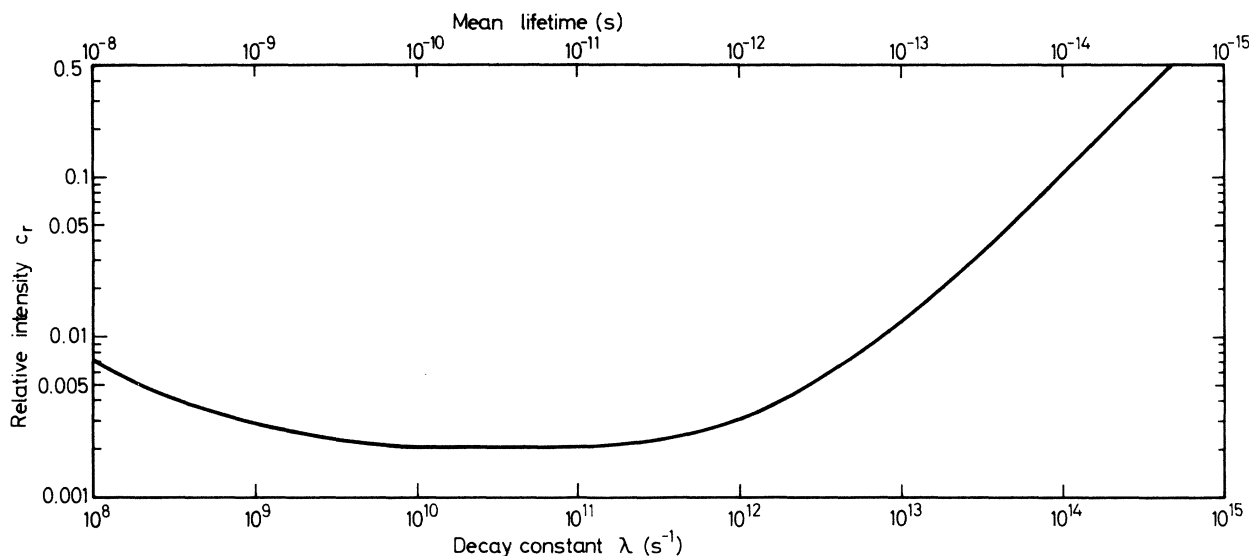


FIG. 4. The upper limit of the relative intensity c_r of a single long-lived component (with a confidence limit of 99.7%) versus the decay constant λ .

and after the fourth step of correction) are shown in Fig. 3. The anisotropies of the original data, and after each step of correction in the energy range 0.18–10.4 MeV, are listed in Table I. The errors correspond to standard deviations and include statistical errors only for the uncorrected result and statistical as well as systematical errors for the final result. The error in the anisotropy due to errors in time zero and resolution function has been estimated to be less than 0.01%. The distance between source and neutron detector has been assigned an error of 0.2 mm, which means an error of 0.04% in the solid angle and in the anisotropy. The angle of nominally 180° between the two positions has been assigned an error of 0.7° , which implies an error of less than 0.01% in the anisotropy. An error of 0.03% in the correction of the difference in the attenuation in the forward and backward directions has been estimated from the cross sections.¹¹

When corrected neither the anisotropies for different energy intervals, cf. Fig. 3, nor the integrated anisotropies, see Table I, are significantly different from zero, and give therefore no positive evidence for neutron emission at longer times. The resulting anisotropy for the energy range 0.18–10.4 MeV, $A = (-0.90 \pm 0.72) \times 10^{-3}$, can be compared with the anisotropy calculated through the

model for different mean lifetimes τ and relative intensities c_r , and an upper limit of the relative intensity of a component with a given mean lifetime and for a given confidence limit can thus be set (see Fig. 4).

V. CONCLUSIONS

A search for neutron emission in the time range 10^{-15} – 10^{-8} s has been made by a method based upon the solid angle aberration. No positive evidence for neutron emission in this time range has been found. With a confidence limit of 99.7% the upper limit of the relative intensity of a component with a given mean lifetime has been derived in the range 2×10^{-15} – 10^{-8} s. The upper limit of the relative intensity reflects the sensitivity of the method as a function of the mean lifetime, and is 11% for a value of the mean lifetime of 10^{-14} s, 1.3% for 10^{-13} s, 0.3% for 10^{-12} s, 0.2% for 10^{-11} – 10^{-10} s, 0.3% for 10^{-9} s and 0.7% for 10^{-8} s. Similar measurements for γ rays⁴ gave the result that 11% of the γ rays are emitted within 10^{-13} s after fission, and it can thus not be excluded that neutrons and γ rays are emitted in the same time region, 10^{-14} – 10^{-13} s.

Thanks are due Dr. T. Sikkeland for supplying the ^{252}Cf source and to Mr. L. Tressum for writing a decoding program for paper tape.

¹V. P. Eismont, *At. Energ.* **19**, 113 (1965).

²K. Skarsvåg, *Phys. Scr.* **7**, 160 (1973).

³J. R. Grover and J. Gilat, *Phys. Rev.* **157**, 814 (1967); T. D. Thomas and J. R. Grover, *ibid.* **159**, 980 (1967).

⁴K. Skarsvåg, *Nucl. Phys.* **A253**, 274 (1975).

⁵V. N. Nefedov, A. K. Melnikov, and B. I. Starostov, in *Proceedings of a Consultants' Meeting on Prompt Fission Neutron Spectra, Vienna, 1971* (IAEA, Vienna

1972), p. 89.

⁶L. Jeki, G. Kluge, and A. Lajtai, Report No. KFKI-71-35, 1971 (unpublished).

⁷P. P. Dyachenko, V. M. Piskaikin, and A. Lajtai, *Yad. Fiz.* 19, 1212 (1974) [*Sov. J. Nucl. Phys.* 19, 619 (1974)].

⁸J. S. Fraser, *Phys. Rev.* 88, 536 (1952).

⁹H. R. Bowman, S. G. Thompson, J. C. D. Milton, and W. J. Swiatecki, *Phys. Rev.* 126, 2120 (1962).

¹⁰E. R. Rae and E. M. Bowey, *Proc. Phys. Soc.* 66A, 1073 (1953).

¹¹*Neutron Cross Sections*, compiled by D. I. Garber and R. R. Kinsey, Brookhaven National Laboratory Report No. BNL-325 (National Technical Information Service, Springfield, Virginia, 1976), 3rd ed., Vol. II, Curves, pp. 62, 63, 69, 70, 158-160.